Journal of Alloys and Compounds 509 (2011) L187–L193

Contents lists available at ScienceDirect

Journal of Alloys and Compounds

journal homepage: www.elsevier.com/locate/jallcom

Letter

Structure stability and mechanical properties of Mg–Al-based alloy modified with Y-rich and Ce-rich misch metals

Jinghuai Zhang[a], Zhe Leng[a], Shujuan Liu[b], Milin Zhang[a,*], Jian Meng[c], Ruizhi Wu[a]

[a] Key Laboratory of Superlight Materials & Surface Technology, Ministry of Education, Harbin Engineering University, Harbin 150001, China
[b] Department of Materials Physics and Chemistry, Harbin Institute of Technology, Harbin 150001, China
[c] State Key Laboratory of Rare Earth Resources Utilization, Changchun Institute of Applied Chemistry, Chinese Academy of Sciences, Changchun 130022, China

ARTICLE INFO

Article history:
Received 28 December 2010
Received in revised form 24 February 2011
Accepted 28 February 2011
Available online 8 March 2011

Keywords:
Mg–Al–RE alloy
$Al_{11}RE_3$
Thermal stability
Mechanical properties

ABSTRACT

Mg–3.4 wt.% Al-based alloy modified with 2.4 wt.% Ce-rich and 0.3 wt.% Y-rich misch metals was prepared by high-pressure die-casting. The microstructure, thermal stability of intermetallic phases and mechanical properties were investigated. The cross-section of test bar is divided into the fine skin region and the wide core region by a narrow band. Two intermetallic phases $Al_{11}RE_3$ and Al_2RE, with the former being the dominant one, are mainly distributed at the interdendritic regions. The $Al_{11}RE_3$ intermetallics possess high volume fraction, fine acicular/lamellar morphology and layered arrangement. It is suggests that each rare earth element has the individual preference for the above two Al–RE intermetallics. The thermal stability of $Al_{11}RE_3$ is conditioned. It is basically stable at temperature up to 200 °C within 800 h, while almost all $Al_{11}RE_3$ intermetallics transform to Al_2RE at higher temperature of 450 °C for 800 h. The alloy exhibits remarkably improved tensile and compressive yield strengths at room temperature and 200 °C and they are the results of the reinforcement of dendrite boundaries with $Al_{11}RE_3$ intermetallics, the fine dendritic arm spacing effect as well as the solid solution strengthening with various rare earth elements.

1. Introduction

As the lightest metal structural material, magnesium alloy is very suitable for the automotive industry where weight saving, energy efficiency and emission reduction are essential at present [1]. Majority of magnesium parts used in automotive applications is high-pressure die-cast (HPDC). The HPDC Mg–Al-based alloys such as AZ91D, AM60B and AM50A alloys are used extensively since these alloys exhibit good die castability and suitable balance of room-temperature strength and ductility [1,2]. However, the application temperature of these alloys is limited to about 125 °C, above which the mechanical properties decrease sharply [3].

The design of alloys for good heat resistance has to be based on an understanding of what the strengthening mechanisms are, how they fail and how their failure can be retarded [4]. A widely accepted view is that both diffusion controlled dislocation climb and grain boundary sliding (GBS) are the creep mechanism in Mg alloys [3,5]. Moreover, Moreno et al. [6] has pointed out that microstructural instability in the near-grain boundary regions significantly influences creep behavior in the fine-grained HPDC Mg alloys. Up to now, typical heat resistant HPDC Mg alloys developed include AE42 (Mg–4Al–2RE) [7], AE44 (Mg–4Al–4RE) [8], MEZ (Mg–2RE–0.3Zn) (above RE = Ce-rich misch metal) [6], AJ62 (Mg–6Al–2Sr) [9], AX52 (Mg–5Al–2Ca) [10] and MRI153 (Mg–9Al–0.7Zn–1Ca–0.1Sr) [11]. The strengthening mechanism of these alloys mainly focused on the reinforcement of grain/dendrite boundaries with thermally stable intermetallic particles to inhibit GBS. However, some intermetallics are not always thermal stable just as $Mg_{17}Al_{12}$ in AZ and AM alloys. They either undergo phase transition or small ones disappear and larger ones grow [4]. On the other hand, the hard intermetallics can increase strength and the influencing degree is dependent on the characteristics of the intermetallics such as type, size, morphology and distribution [12].

In fact, to improve highly heat resistant Mg alloys, besides grain/dendrite boundaries the strengthening of Mg matrix by solid solution and/or precipitation also should give consideration. Maruyama et al. [13] reported that Y has a higher solid solution strengthening effect than Al in Mg alloys. Just recently, Zhu et al. [14] studied the relationship between microstructure and creep resistance in HPDC Mg–La, Mg–Ce, Mg–Nd binary alloys and reported that strengthening of the α-Mg matrix by solid solution and/or precipitation is more important than grain boundary reinforcement by intermetallic phases for creep resistance of HPDC Mg–RE alloys.

The behavior of RE elements in Mg alloys can be divided into two subgroups: the Ce subgroup and the Y subgroup [15]. The solid

* Corresponding author. Tel.: +86 451 82533026; fax: +86 451 82533026.
E-mail address: jinghuaizhang@gmail.com (M. Zhang).

0925-8388/$ – see front matter © 2011 Elsevier B.V. All rights reserved.
doi:10.1016/j.jallcom.2011.02.173

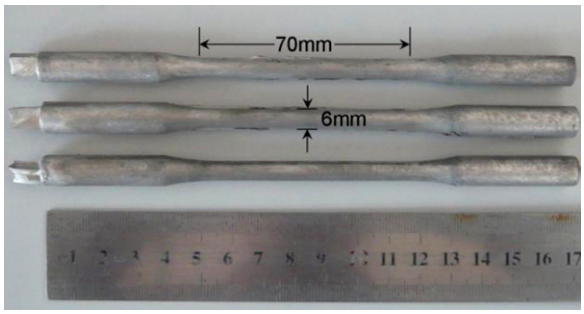

Fig. 1. HPDC tensile test bars obtained from AEW320.

solubility of the formers in Mg is low while it is high for the latters. In addition, RE additions have generally been regarded as expensive alloying additions, but in fact Ce-rich misch metal (Cemm) containing most of Ce subgroup elements and Y-rich misch metal (Ymm) composed of most Y subgroup elements are relatively low in cost and much cheaper than the single rare earth [16,17]. In this work, a new heat-resistant HPDC Mg alloy was designed. Relatively low Al content was used to improve the die castability and form high melting point Al–RE intermetallics; Cemm with the low solid solubility in Mg was added to form large amount of intermetallic particles to reinforce the grain/dendrite boundaries; Ymm with high solubility in Mg was expected to provide strengthening of the α-Mg matrix. As for this paper, we mainly focused on the microstructure, thermal stability of intermetallic and mechanical properties at room temperature and 200 °C of HPDC Mg–Al–Cemm–Ymm-based alloy.

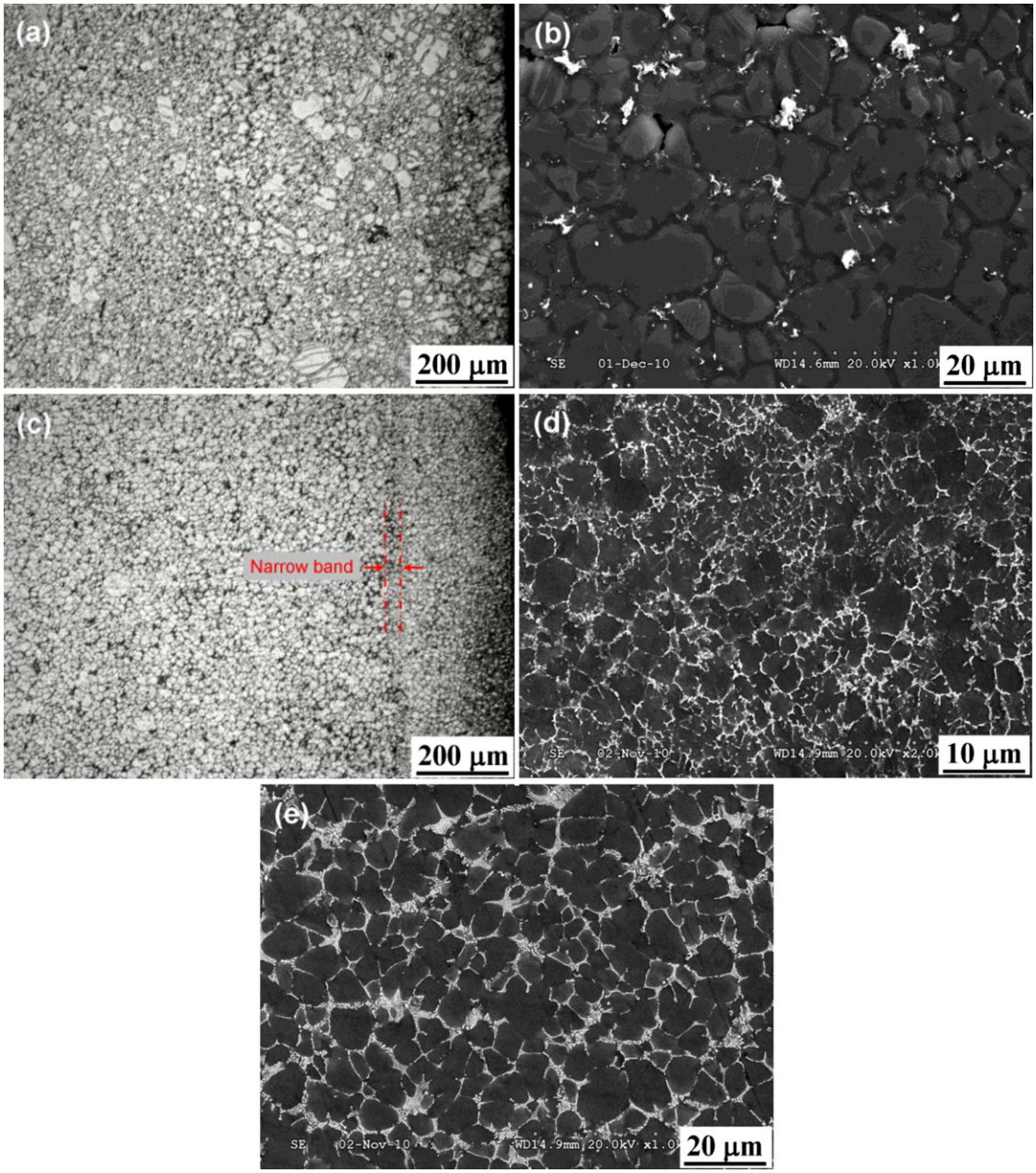

Fig. 2. Microstructure of the HPDC alloys: (a) OM image showing the skin and partial core regions of AM30; (b) SEM image showing the core regions of AM30; (c) OM image showing the skin and partial core regions of AEW320; SEM images showing the skin (d) and core (e) regions.

Table 1
Main chemical compositions of the Ce-rich misch metal and Y-rich misch metal.

Misch metal	Composition (wt.%)												
	La	Ce	Pr	Nd	Sm	Eu	Dy	Ho	Er	Tm	Yb	Lu	Y
Cemm	27.03	51.46	5.87	15.64	<0.10	–	–	–	–	–	–	–	–
Ymm	0.11	–	–	0.16	–	<0.10	0.11	6.30	11.22	1.45	0.18	0.55	79.75

2. Experimental procedures

The chemical composition (wt.%) of experimental alloy is Mg–3.4Al–2.4Cemm–0.3Ymm–0.3Mn (AEW320). The reference alloy prepared and tested in the same condition is Mg–3.3Al–0.2Mn (AM30). Commercial pure Mg and Al were used, Mn, Cemm and Ymm were added in the form of Al–10 wt.% Mn and Mg–20 wt.% Cemm and Mg–20 wt.% Ymm master alloys, respectively. Specimens were produced using a 280 t clamping force cold chamber die-cast machine. The main chemical compositions of the misch metals and the specimens were determined by inductively coupled plasma atomic emission spectroscopy (ICP-AES). Table 1 lists the main compositions of Cemm and Ymm. Only the Ce and Y contents were analysed in the specimens and the rest rare earth elements were calculated according to the composition of misch metals.

The tensile samples were 70 mm in gauge length and 6 mm in gauge diameter, as shown in Fig. 1. The compressive samples were 6 mm in diameter and 10 mm in height, which were cut from the tensile bars. Tensile and compressive tests were performed using Instron 5869 tensile testing machine with a strain rate of 1.1×10^{-3} s^{-1}. The value in the study was the average of at least four measurements. Metallographic samples were cut from the middle segment of the tensile bars. The microstructure and intermetallic phases were characterized by scanning electron microscope (SEM) equipped with an energy dispersive X-ray spectrometer (EDS) and X-ray diffraction (XRD).

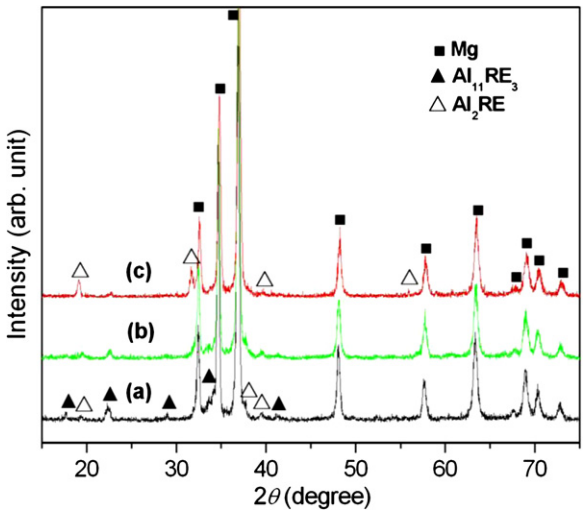

Fig. 3. XRD patterns of the HPDC AEW320 alloy (a), the samples after annealing at 200 °C (b) and 450 °C (c) for 800 h.

3. Results and discussion

3.1. Microstructure

In order to study the role of the Cemm and Ymm additions in the Mg–3Al-based alloy, firstly the microstructure of HPDC AM30 alloy without Cemm and Ymm is shown in Fig. 2(a) and (b). It reveals that the AM30 alloy consists of the primary α-Mg dendrites surrounded with interdendritic eutectic. Moreover, there is no obvious compact layer in skin region. Further SEM observation reveals that the average dendritic arm spacing (DAS) is about 17 μm and a spot of β-$Mg_{17}Al_{12}$ intermetallics disperse in interdendritic regions. The obvious changes in the microstructure can be observed with Cemm and Ymm additions. As shown in Fig. 2(c), a narrow band can be found and divides the cross-section into the skin region with the thickness of about 200 μm and the wide core region. Peng et al. [18] identified that the similar narrow band in HPDC Mg–Gy–Dy alloy is the segregation of the alloying elements. What is more important, the amount of intermetallic compounds in interdendritic regions in AEW320 alloy is much higher than that in AM30 alloy of similar Al content. Fig. 2(d) and (e) shows the comparative observation on the skin region and core region microstructures. It can be seen that the skin region has the much finer dendrites than the core region of the casting. The average DAS in skin region is less than 3 μm while the value of the core region is up to 8 μm.

3.2. Intermetallics and their thermal stability

XRD result of the HPDC AEW320 alloy is illustrated in Fig. 3(a). It has been known that AZ and AM alloys are mainly composed of α-Mg and β-$Mg_{17}Al_{12}$ phases, while as shown in the figure, no obvious peaks of β-$Mg_{17}Al_{12}$ phase emerge due to the addition of Cemm and Ymm. The main secondary phases in AEW320 alloy are $Al_{11}RE_3$ and Al_2RE (RE here represents both Cemm and Ymm), while $Al_{11}RE_3$ diffraction peak is much more intense than that of Al_2RE, which suggests that the former is the dominant secondary phase.

The magnified SEM images characterizing the secondary phases in the core region of HPDC AEW320 alloy are shown in Fig. 4. It can be found that the acicular/lamellar intermetallics with the length of 1–3 μm arrange in a row then the rows form layers roughly (Fig. 4(a) and (b)). This is the outstanding morphology and distribution of the intermetallics. EDS analyses were used to identify these intermetallics. Fig. 4(d) shows one of the EDS spectrums and Table 2 lists the elementary compositions (marked as A). Note that almost all the rare earth elements within Cemm and Ymm are detected and Ce content is most among them. Combined with XRD result, the acicular/lamellar intermetallics are identified as $Al_{11}RE_3$. Besides, a few quadrate-like intermetallics with size of 1–3 μm can be found by careful SEM observations, as shown in Fig. 4(c). Fig. 4(e) dis-

Table 2
EDS analysis results of acicular/lamellar (A) and quadrate-like (B) intermetallics.

Phase	Composition (at.%)													
	Mg	Al	Ce	La	Y	Nd	Ho	Sm	Dy	Lu	Eu	Er	Tm	Mn
A	79.35	15.80	1.74	1.02	0.92	0.35	0.16	0.13	0.12	0.11	0.10	0.08	–	0.11
B	76.23	15.08	1.21	0.14	6.43	0.18	0.22	0.02	–	0.07	0.11	0.17	0.09	0.06

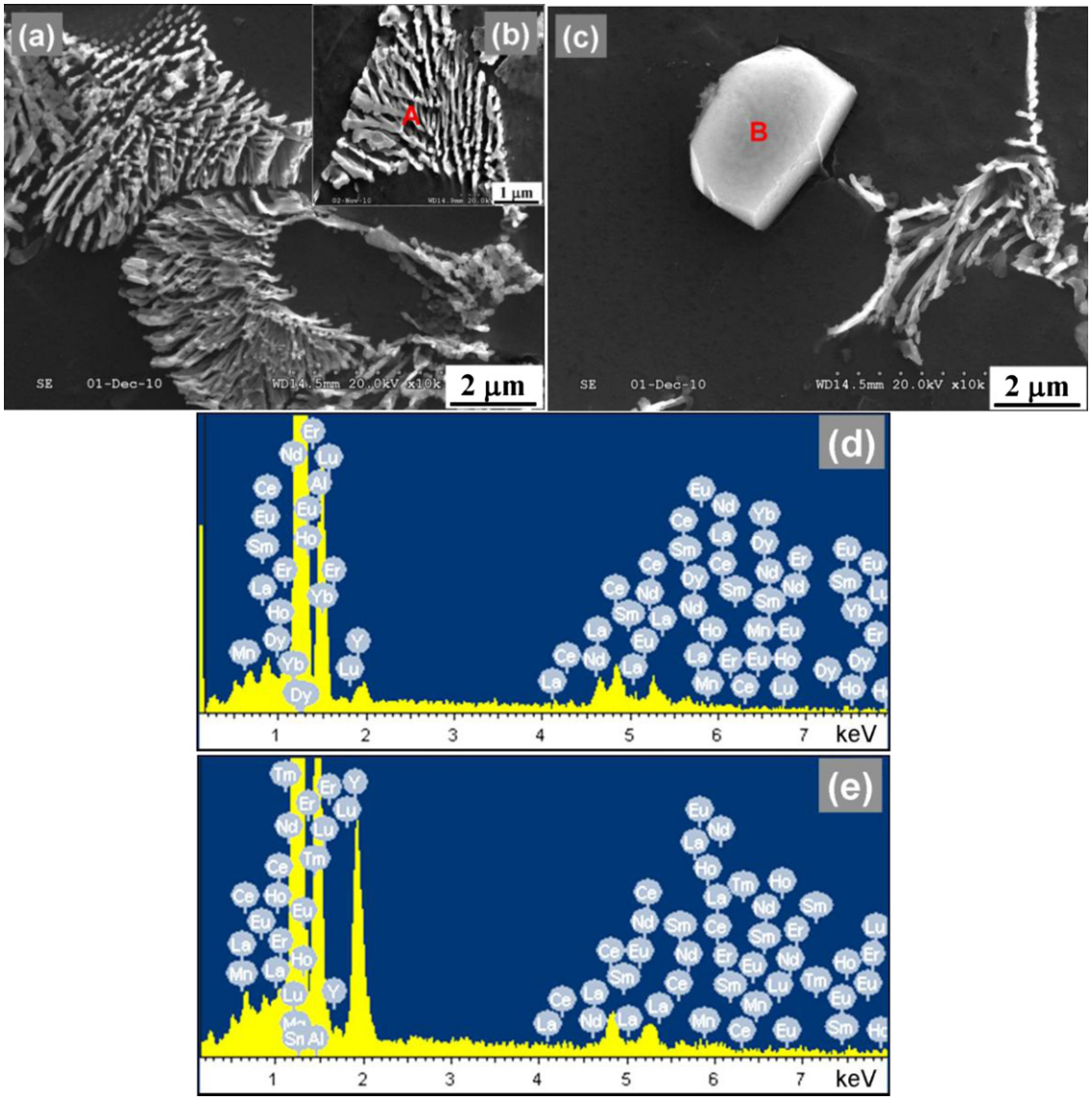

Fig. 4. (a)–(c) SEM images of the intermetallic phases in HPDC AEW320 alloy; (d) EDS spectrum of acicular/lamellar intermetallics; (e) EDS spectrum of quadrate-like intermetallic.

plays one of its EDS spectrums and the elementary compositions are also listed in Table 2 (marked as B). It is worthwhile to note that Y content is much higher than the other rare earth elements. The quadrate-like intermetallic corresponds to Al_2RE according to EDS analyses combined with the XRD result. Here some cases should be pointed out in the EDS analyses. The interaction between the electron beam and the Mg matrix is inevitable due to the so fine size of the particles, thus Mg atoms are found in the EDS analyses. The content of some rare earth elements with low level in Cemm and Ymm are not determined completely in the intermetallics and their relative proportions are alterable, while the ratio of main rare earth elements such as Ce, La, Y and Nd are almost certain.

To study the thermal stability of Al–RE intermetallics, some samples were annealed at 200 °C and 450 °C for 800 h, respectively. The microstructure of AEW320 alloy after annealing treatment is shown in Fig. 5. In 200 °C annealing sample, as shown in Fig. 5(a) and (b), the acicular/lamellar $Al_{11}RE_3$ intermetallics in the interdentritic regions appear to be stable, without discernible change in size or shape. Careful examination reveals an interesting feature as shown in Fig. 5(c), a cubic Al_2RE intermetallic grows together with the dendritic $Al_{11}RE_3$. XRD patterns also show incognizable changes before and after 200 °C annealing by compared Fig. 3(a) with (b). However, the obvious change of microstructure could be observed after annealing treatment at higher temperature of 450 °C (Fig. 5(d)). At higher magnification as shown in Fig. 5(e) and (f), it reveals that almost all the acicular/lamellar intermetallics disappear and give place to fine quadrate-like particles with size of about 100–300 nm in interdendritic regions. XRD pattern as shown in Fig. 3(c) also changes obvious after annealing at 450 °C, namely, the intensity of $Al_{11}RE_3$ peaks decrease and that of Al_2RE peaks increase obviously. It is a significant observation, which gives the clear evidence of $Al_{11}RE_3$ phase transition.

However, the stability and decomposition of the main strengthening phase $Al_{11}RE_3$ in Mg–Al–RE-based alloys are still a matter of debate in the previous reports. According to the earlier work by Powell et al. (AE42, 175 °C for 1000 h with and without stress) [19]

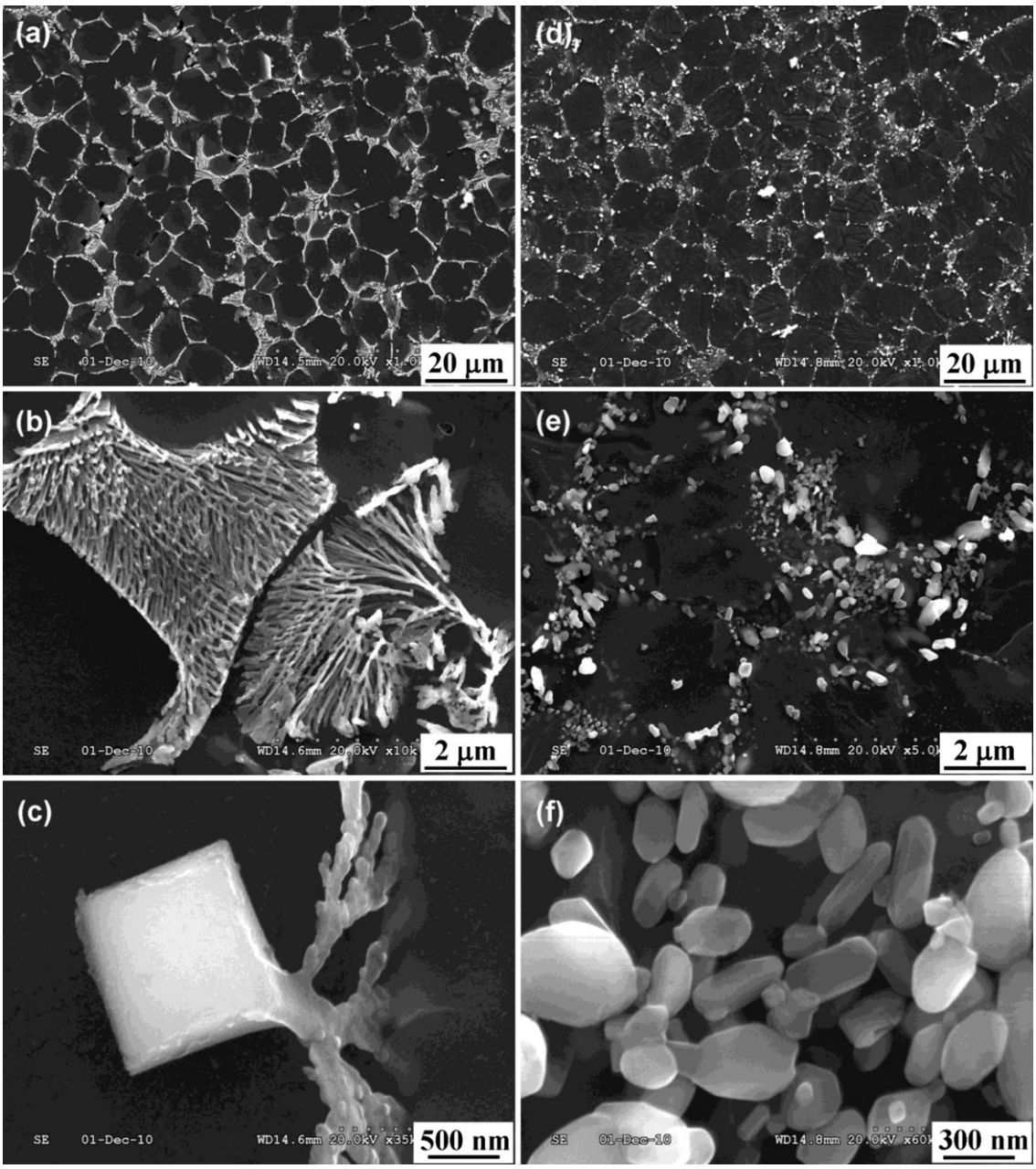

Fig. 5. SEM images showing microstructure of HPDC AEW320 alloy after annealing at (a)–(c) 200 °C and (d)–(f) 450 °C for 800 h.

and our recent work (AE44, 200 °C for 100 h with 70 MPa stress) [20], $Al_{11}RE_3$ is unstable and partially decomposes to Al_2RE. In contrast, Pettersen et al. (AE42 heat treated at 150, 200 and 250 °C for 100 h) [21], Huang et al. (AE42, 450 °C for 15 h) [7], Zhu et al. (AE42, 200 °C for 2 weeks) [22], Dargusch et al. (AE42 + 1 wt.% Sr, 200 °C for 2 weeks) [23], Rzychoń et al. (AE44, 175 °C for 3000 h) [24] and Shang et al. (AZ31 + 0.21 wt.% Ce, 450 °C for 10 h) [25] reported that the intermetallic phase $Al_{11}RE_3$ have high thermal stability, without decomposition observed. The observations reported here indicate that there is a limit to the thermal stability of $Al_{11}RE_3$, and it is stable at temperature up to 200 °C within 800 h, while almost all $Al_{11}RE_3$ intermetallics transform to Al_2RE at higher temperature of 450 °C for 800 h. As to the exact phase transition point (temperature and time) and the effect of different rare earth elements in $Al_{11}RE_3$ on its stability, further work would be required.

3.3. Mechanical properties

The representative tensile and compressive stress–strain curves of HPDC AEW320 and AM30 alloys at room temperature (RT) and 200 °C are shown in Fig. 6. Table 3 lists the tensile properties including tensile yield strength (TYS), ultimate tensile strength (UTS) and tensile elongation (ε_t) and the compressive properties including compressive yield strength (CYS), ultimate compressive strength (UCS) and compressive elongation (ε_c). Two notable informations can be obtained by analysis of these figures and data. The strength increases dramatically by about 40–75 MPa while the elongation still keeps similar level with adding Cemm and Ymm to AM30 alloy.

The following aspects are considered to be related to the improved strength. Since the DAS is finer for the Mg–3Al-based alloys with Cemm and Ymm, the fine DAS effect can contribute to the observed increase in strength. Another factor to be considered

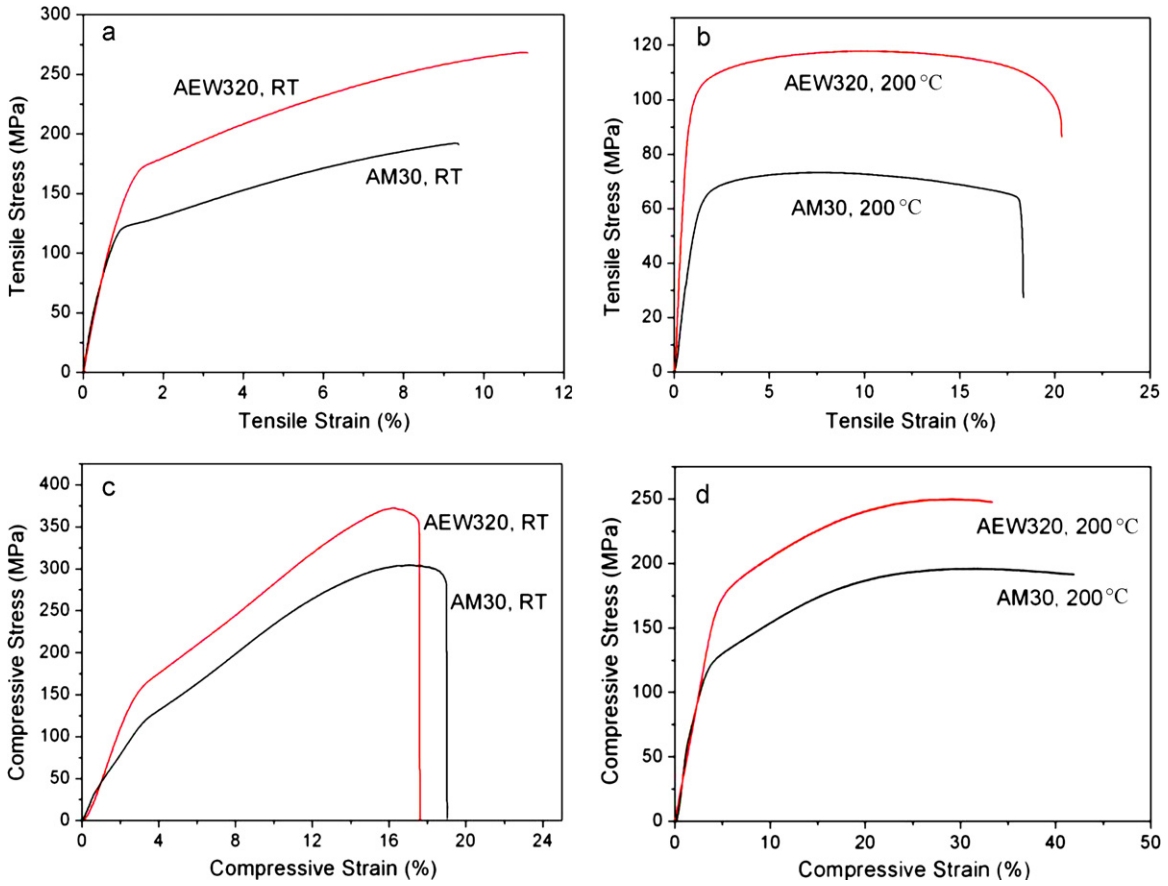

Fig. 6. Typical stress–strain curves of the HPDC alloys: (a) tensile curves at (a) room temperature and (b) 200 °C; compressive curves at (c) room temperature and (d) 200 °C.

Table 3
Tensile and compressive properties of the HPDC alloys at room temperature and 200 °C.

Alloy	RT			200 °C			RT			200 °C		
	TYS (MPa)	UTS (MPa)	ε_t (%)	TYS (MPa)	UTS (MPa)	ε_t (%)	CYS (MPa)	UCS (MPa)	ε_c (%)	CYS (MPa)	UCS (MPa)	ε_c (%)
AEW320	166	267	11	102	117	20	158	372	17	169	249	33
AM30	116	191	9	60	72	18	115	305	19	113	195	41

is the strengthening of the α-Mg matrix by solid solution with various rare earth elements. The last and also the more important is the formation of large amount of $Al_{11}RE_3$ intermetallics which provide the considerable reinforcement of dendrite boundaries. Generally, the ductility is low for the alloy containing a large number of intermetallic particles [26]. However, the elongation of HPDC AEW320 alloy with high volume fraction of intermetallics still keeps high level as that of AM30 alloy. It may be attributed to the fine morphology and arrangement of $Al_{11}RE_3$ intermetallics.

4. Conclusions

The microstructure, intermetallic phases and mechanical properties of high-pressure die-cast Mg–3.4Al–2.4Cemm–0.3Ymm–0.3Mn (wt.%, Cemm = Ce-rich misch metal, Ymm = Y-rich misch metal) alloy have been investigated. The main results are summarized as follows.

(1) The cross-section of test bar could be divided into the fine skin region and the wide core region. A large amount of $Al_{11}RE_3$ intermetallics with fine acicular/lamellar morphology and layered arrangement and a few quadrate-like Al_2RE were observed at the interdendritic regions. Ce content in $Al_{11}RE_3$ is higher than the other rare earth elements and Y is preferred to exist in Al_2RE.
(2) Both the $Al_{11}RE_3$ and Al_2RE intermetallics are stable at temperature up to 200 °C within 800 h, while almost all $Al_{11}RE_3$ transform to Al_2RE at higher temperature of 450 °C for 800 h. This suggests that the thermal stability of $Al_{11}RE_3$ is conditioned.
(3) The alloy exhibits significantly improved tensile and compressive strengths at room temperature and 200 °C, which is mainly attributed to the reinforcement of dendrite boundaries with $Al_{11}RE_3$ intermetallics, the small dendritic arm spacing effect as well as the solid solution strengthening with various rare earth elements.

Acknowledgements

This work was supported by the Fundamental Research funds for the Central Universities (HEUCF101008), the Key Project of Science and Technology of Harbin City (2010AA4BE031), the Project of Science and Technology of Heilongjian Province Education Department (11553054), the China Postdoctoral Science Founda-

tion (20100471015, 20100471046), the Heilongjiang Postdoctorial Fund (LBH-Z09217) and the Natural Scientific Research Innovation Foundation in Harbin Institute of Technology (HIT.NSRIF.2009026).

References

[1] M.K. Kulekei, Int. J. Adv. Manuf. Technol. 39 (2008) 851–865.
[2] H. Giestland, H. Westengen, Adv. Eng. Mater. 9 (2007) 769–776.
[3] B.H. Kim, S.W. Lee, Y.H. Park, I.M. Park, J. Alloys Compd. 493 (2010) 502–506.
[4] O. Mihriban, Pekguleryuz, Mater. Sci. Forum 350–351 (2000) 131–140.
[5] A.A. Luo, Int. Mater. Rev. 49 (2004) 13–30.
[6] I.P. Moreno, T.K. Nany, J.W. Jones, J.E. Allison, T.M. Pollock, Scripta Mater. 48 (2003) 1029–1034.
[7] Y.D. Huang, H. Dieringa, N. Hort, P. Maier, K.U. Kainer, Y.L. Liu, J. Alloys Compd. 463 (2008) 238–245.
[8] P. Bakke, H. Westengen, Magnesium Technol. 12 (2005) 291–296.
[9] G. L'Espérance, P. Plamondon, M. Kunst, A. Fischersworring-Bunk, Intermetallics 18 (2010) 1–7.
[10] Y. Terada, T. Sato, J. Alloys Compd. 504 (2010) 261–264.
[11] S.M. Zhu, B.L. Mordike, J.F. Nie, Metall. Mater. Trans. A 37 (2006) 1221–1229.
[12] J. Zhang, Z. Leng, M. Zhang, J. Meng, R. Wu, J. Alloys Compd. 509 (2011) 1069–1078.
[13] K. Maruyama, M. Suzuki, H. Sato, Metall. Mater. Trans. A 33 (2002) 875–882.
[14] S.M. Zhu, M.A. Gibson, M.A. Easton, J.F. Nie, Scripta Mater. 63 (2010) 698–703.
[15] B. Smola, I. Stulíková, J. Pelcová, B.L. Mordike, J. Alloys Compd. 378 (2004) 196–201.
[16] J. Zhang, X. Niu, X. Qiu, K. Liu, C. Nan, D. Tang, J. Meng, J. Alloys Compd. 471 (2009) 322–330.
[17] J.H. Zhang, H.F. Liu, W. Sun, H.Y. Lu, D.X. Tang, J. Meng, Mater. Sci. Forum 561–565 (2007) 143–146.
[18] Q. Peng, L. Wang, Y. Wu, L. Wang, J. Alloys Compd. 469 (2009) 587–592.
[19] B.R. Powell, V. Rezhets, M.P. Balogh, R.A. Waldo, JOM-J Min. Met. Mater. S 54 (2002) 34–38.
[20] J.H. Zhang, P. Yu, K. Liu, D.Q. Fang, D.X. Tang, J. Meng, Mater. Des. 30 (2009) 2372–2378.
[21] G. Pettersen, H. Westengen, R. Hoier, O. Lohne, Mater. Sci. Eng. A 207 (1996) 115–120.
[22] S.M. Zhu, M.A. Gibson, J.F. Nie, M.A. Easton, T.B. Abbott, Scripta Mater. 58 (2008) 477–480.
[23] M.S. Dargusch, S.M. Zhu, J.F. Nie, G.L. Dunlop, Scripta Mater. 60 (2009) 116–119.
[24] T. Rzychoń, A. Kielbus, J. Cwajna, J. Mizera, Mater. Charact. 60 (2009) 1107–1113.
[25] L. Shang, I.H. Jung, S. Yue, R. Verma, E. Essadiqi, J. Alloys Compd. 492 (2010) 173–183.
[26] D.H. Bae, S.H. Kim, D.H. Kim, W.T. Kim, Acta Mater. 50 (2002) 2343–2356.